Langmuir Monolayers of Monodispersed Magnetic Nanoparticles Coated with a Surfactant

S. Lefebure, C. Ménager, and V. Cabuil

Equipe Colloïdes Magnétiques, Laboratoire LI2C, UMR 7912 associée au CNRS et à l'Université Pierre et Marie Curie, 4, place Jussieu, 75252 Paris Cedex 05, France

M. Assenheimer† and F. Gallet*

Laboratoire de Physique Statistique de l'Ecole Normale Supérieure, URA 1306 associée au CNRS et aux Universités Paris 6 et Paris 7, 24, rue Lhomond, 75231 Paris Cedex 05, France

C. Flament

Equipe ferrofluides, UFR de physique, Université Paris 7, Denis Diderot, 2, place Jussieu, 75251 Paris Cedex 05, France

Received: December 3, 1997

Monolayers of hydrophobic magnetic nanoparticles are deposited on a water subphase in a Langmuir trough. The shape of the surface isotherms and the electron-micrograph pictures appear to be strongly dependent on the particle size. Small particles are organized in more compact aggregates than larger ones. We interpret this behavior as a size-dependent balance between van der Waals and magnetic interparticle interactions.

Introduction

Associations of magnetic nanoparticles with self-assembled surfactant structures, especially with bilayers, have been reported in various configurations. For instance, nanoparticles have been confined in lamellar systems[1,2] and in vesicles or liposomes.[3,4] The usual process to elaborate such hybrid systems is to mix the lyotropic system with a magnetic fluid, which is a colloidal dispersion of magnetic nanoparticles in water or in an oily solvent.[5]

The existence of a hybrid magnetic colloid may be expressed in terms of osmotic-pressure equilibrium.[2] In three-dimensional systems, a magnetic fluid is usually described as a gas of particles interacting through an anisotropic potentiel, taking into account the van der Waals attractions, the dipolar magnetic interactions, and the short-range repulsions. Phase transitions that are gas−liquid-like have been observed and studied in such systems.[6]

A few years ago, Fendler et al. described a way to prepare magnetic particle monolayers on a water subphase.[7] This pioneering work showed that it is possible to obtain uniform monolayers of magnetic nanoparticles. The authors noticed a weak effect of particle size on the electron micrographs, but since the system was polydisperse, this effect was hardly interpretable.

In this work, we study monolayers of monodisperse magnetic nanoparticles, surfactant-coated, spread on a water subphase. We especially investigate the effect of particle size on the electron micrographs and on the shape of the compression isotherms. For all particle sizes, dense, single-layered aggregates are visible with an optical microscope. Electron micrographs show that, at the particle length scale, the domains are rather compact for small particles (7.5 nm in diameter), while they are more digitated and behave like an elastic gel for larger ones (15.5 nm in diameter). We propose an interpretation of this effect in terms of interparticle interactions. Preliminary results in a nonzero magnetic field are also presented.

Experimental Section

All chemicals are of reagent grade purchased from PROLABO and used without further purification. The subphase is ultrapure deionized water (from a Millipore Milli-Q apparatus), alkalinized to pH = 10 by NaOH addition (from MERCK, purissimum).

Magnetic Nanoparticles. Particles are maghemite grains (γ-Fe_2O_3). They are prepared according to Massart's method[8] by alkalinization with ammonia at room temperature of aqueous mixtures of ferric and ferrous salts in a molar ratio of 2:1. The magnetite particles thus obtained are very reactive toward acid attack and air oxidation. Thus, a controlled chemical oxidation in acidic medium with ferric nitrate is performed in order to get maghemite particles, which are stable for years either in alkaline or in acidic medium. Because of the acid−base behavior of the ferric oxide surface, these particles have cationic surface charges in acidic aqueous solution. These charges ensure electrostatic repulsions between grains, which can be dispersed in water to obtain a stable acidic colloidal solution called ferrofluid.[5] Particle size distribution is usually well described by a log−normal law:

$$p(D) = \frac{1}{\sqrt{2\pi}\,\sigma D} \exp\left[-\frac{1}{2\sigma^2}\left(\ln\frac{D}{D_0}\right)^2\right]$$

where D_0 is the mean diameter and σ the standard deviation. The synthesis leads to polydisperse samples, and a size-sorting procedure has to be performed in order to obtain from the initial dispersion several fractions of almost monodisperse particles.[9]

* To whom correspondence should be addressed. Telephone: 33 1 44 27 68 55. Fax: 33 1 44 27 43 33. E-mail: gallet@lbhp.jussieu.fr.

† Present address: CI Systems, P.O. Box 147, 10551 Migdal HaEmek, Israel.

S1089-5647(98)00403-9 CCC: $15.00
Published on Web 03/26/1998

TABLE 1: Size Characteristics of the Used Samples[a]

	A	B	C
D_0 (nm)	7.5	11	15.5
σ	0.1	0.15	0.2
A_0 (nm^2)	50	105	210

[a] D_0 is the mean diameter of the size distribution as defined in the text. σ is the standard deviation for this distribution. $A_0 = (\sqrt{3}/2)D_0^2$ is the area per particle in the monolayer, assuming a triangular close packing.

This procedure is based on the thermodynamic properties of aqueous dispersions of nanoparticles.[6] It allows us to obtain, from a typical polydisperse preparation, three samples with different mean diameters and reduced polydispersities. The size characteristics of the samples used here are given in Table 1. They are deduced from the analysis of the shape of the magnetization curve of the ferrofluid samples as described in ref 10 or by electron microscopy.

At the end of the size-sorting procedure, the cationic particles, dispersed in nitric acid solution, are coated by surfactant molecules in order to make them hydrophobic. As in the study of Fendler et al.,[7] the surfactant is lauric acid (LA). Adsorption of LA is performed in aqueous medium. An excess of surfactant is mixed with the aqueous dispersion of nanoparticles at 100 °C. A hydrophobic precipitate is obtained, and water is eliminated through magnetic decantation. The precipitate is dispersed in hexane, and a second magnetic decantation is done to eliminate the residual water. The volume fraction of magnetic oxide, deduced from light absorption at 480 nm, is adjusted to (3×10^{-2})% by dilution in hexane.

Langmuir Films. Preparation and Characterization. We spread the film either on a small Langmuir trough (10×6.5 cm^2) mounted on the plate of an optical microscope or on a larger one (15×30 cm^2) designed for Langmuir−Blodgett transfer onto solid support. Both are Teflon coated and temperature-regulated. A motorized Teflon piston allows the film area to vary from about 60 to 15 cm^2 for the small trough and from about 450 to 150 cm^2 for the large one. The surface pressure Π is measured by the Wilhelmy method with a filter paper plate (Riegler and Kierstein apparatus) and recorded together with the area per particle A. The compression or decompression rate

$$\frac{1}{A}\frac{dA}{dt}$$

is usually on the order of 20 mn^{-1}.

The hexane magnetic fluid mother solution is diluted to about 10^{16} particles per liter (about 10^{-5} in volume fraction) and slowly spread on the water subphase; the surface pressure is controlled during spreading to remain below 10 mN/m. When the deposition is too fast, the surface pressure may exceed 25mN/m, and the magnetic monolayer partially collapses. The deposition speed is governed by the dissolution rate of the excess of lauric acid into the subphase. This rate is increased by alkalinization of the water subphase to pH = 10. The total amount of hexane magnetic fluid to be spread is such that the minimum area per particle after compression is on the order of A_0, the area per particle in an ideal triangular close-packed lattice.

On the small trough setup, a roughly homogeneous horizontal or vertical magnetic field can be applied to the film surface by mean of two coils or two permanent magnets (100×150 mm^2). The maximum field intensity is about 50 mT in the vertical direction or 35 mT in the horizontal one. In this case the pressure sensor is shielded with a magnetic alloy sheet to minimize the influence of applied magnetic fields.

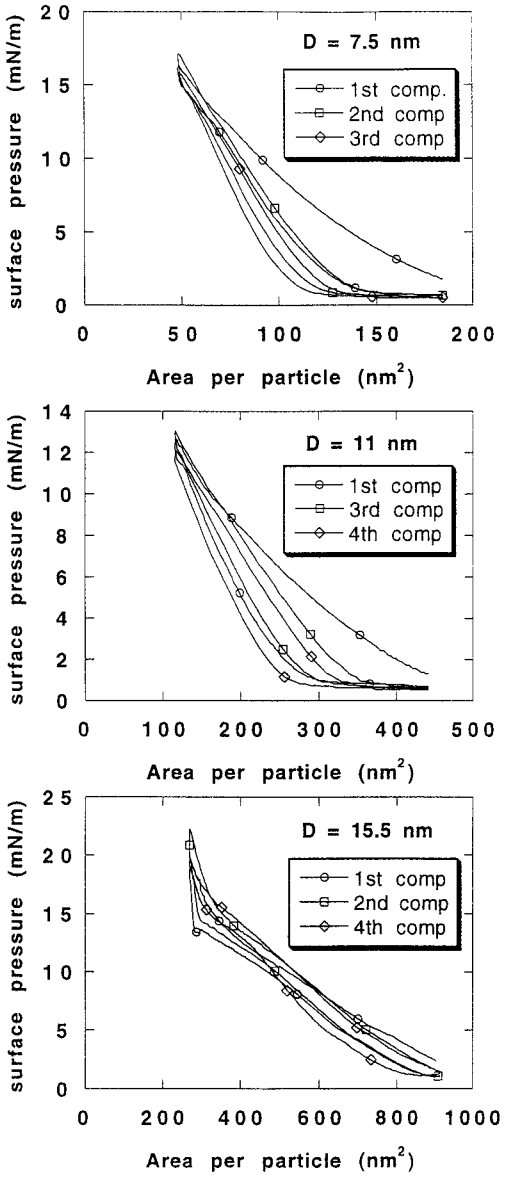

Figure 1. Isotherms $\Pi = f(A)$ at $T = 20$ °C. Π is the surface pressure, A is the area per particle. The particle diameters are (A) 7.5, (B) 10, and (C) 15.5 nm. In each case several compression−expansion cycles are shown. Except for the first cycle (see text), the isotherms are reasonnably reproducible.

During the compression and decompression isotherm recording, the film is observed by reflection through an optical microscope. Owing to the high absorption coefficient of the magnetic particles in the visible range, the difference between the reflection coefficients of pure water and of the interface covered by a dense monolayer is enough to give contrasted images of the layer.[11]

The structure of LB films at the particle scale has also been investigated by transmission electron microscopy. By the usual Langmuit−Blodgett technique, the film has been transferred at different regulated pressures onto an electron grid coated with a thin hydrophilic Formvar layer. This amorphous coating (ca. 160 Å) is obtained by removing a microscope slide from a Formvar solution (1% of Formvar in chloroform) at a constant velocity (0.5 mm s^{-1}). Then the TEM grid is put on a cover

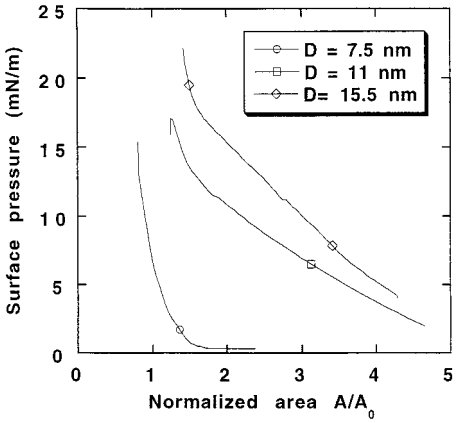

Figure 2. Normalized compression isotherms $\Pi = f(A/A_0)$. A_0 is the area per particle in a close-packed configuration. The particle diameters are (A) 7.5, (B) 10, and (C) 15.5 nm.

glass and covered with the dry Formvar film. Electron micrographs are obtained with a JEOL 100CKII top-entry UHR microscope.

Results

Isotherms $\Pi = f(A)$. The surface pressure Π is plotted as a function of the surface area A per particle for successive compressions and expansions and for the three monodisperse samples of Table 1 (Figure 1). Except for the first compression−expansion cycle, we observe generally reproducible isotherms. For the two smaller sizes (7.5 and 11 nm in diameter) the first isotherm cycle appears to be higher than the following ones. This can be due to some excess lauric acid that solubilizes in the subphase during the first compression. After the first cycle, the compression and expansion isotherms do not exactly superimpose, but this hysteresetic behavior is reproducible and cannot be due to collapse or to some loss of material into the subphase.

The shape of the isotherms depends on the particle size. To better visualize this dependence, we have plotted together in Figure 2 three compression isotherms for the three sample diameters D_0 normalized by the particle area $A_0 = (\sqrt{3}/2)D_0^2$ in an ideal close-packed lattice (Table 1). The isotherms used for normalization are taken from the second compression cycle. These normalized isotherms have very different shapes according to the particle size. For smaller particles (7.5 nm in diameter), the isotherms present a very low-pressure plateau ($\Pi \cong 0$ mN/m) followed by a rapid pressure increase when $A/A_0 \cong 1$. In this region the compression coefficient

$$\alpha = -A\frac{d\Pi}{dA}$$

is about 30mN/m. For larger particles (15.5 nm in diameter), the surface pressure increases more slowly from large to small areas per particle, α is only about 10mN/m, and the low-pressure plateau is shifted to higher areas per particle. In all cases, the pressure starts to increase abruptly when A/A_0 is close to 1, within experimental error. This is consistent with the formation of a dense monolayer, without any solubilization of particles. We observed film collapse at $\Pi \approx 25-30$ mN/m.

Optical Microscopy. The film structure was observed during compression and expansion, using reflection microscopy. Typical images are shown in Figure 3. Bright domains correspond to regions of high particle density, dark ones to low densities. Actually, the intensity in these regions is similar to the pure

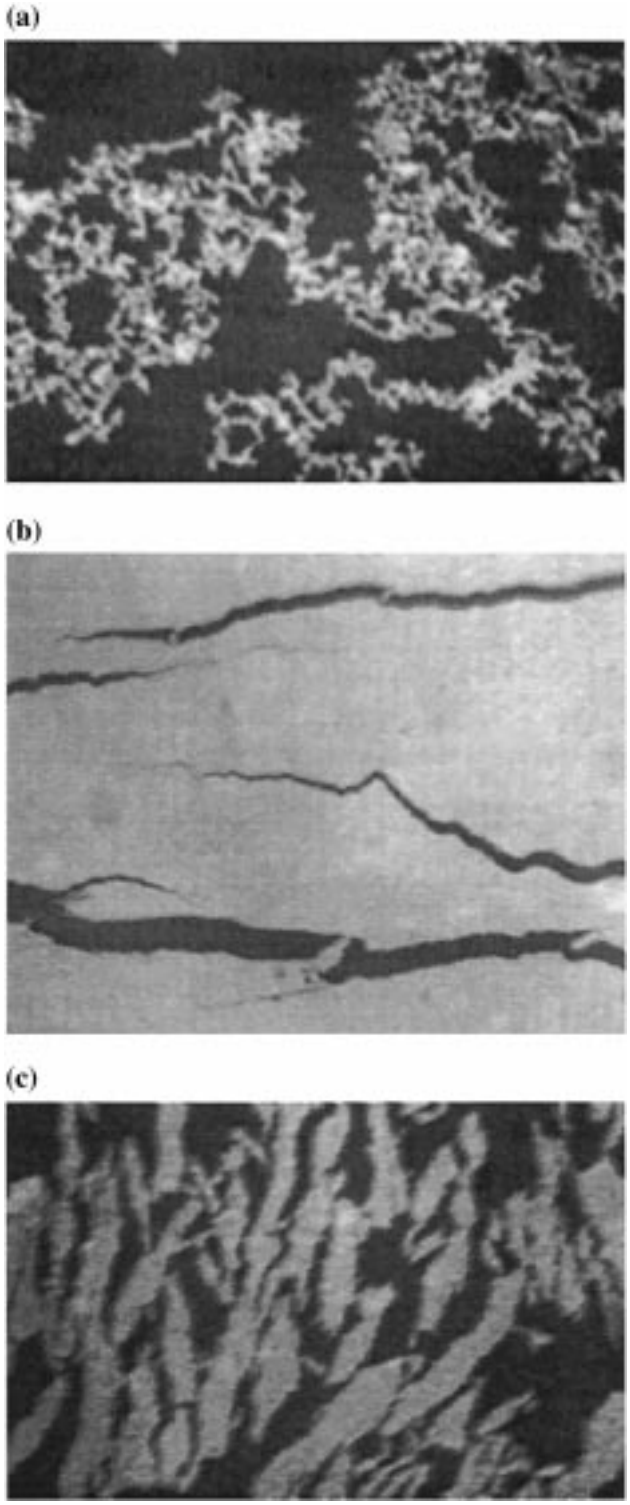

Figure 3. Typical reflection microscopy pictures: (a) 15.5-nm particles right after deposition ($A = 900$ nm^2, $\Pi \approx 0$ mN/m); (b) 7.5-nm particles during decompression ($\Pi = 3$ mN/m); (c) 15.5-nm particles after a first compression−decompression cycle ($\Pi \approx 0$ mN/m).

air/water interface. Thus, we consider that the particle density is very small, or nearly zero, out of the bright domains. Right after deposition, for all particle sizes, and at low pressure, most of the particles are condensed in macroscopic digitated aggregates (Figure 3a). During the first compression, these aggregates become more and more compact. Finally, at the maximum density ($A/A_0 \cong 1$) the film appears uniformly bright, meaning that the particles form a homogeneous monolayer of constant thickness. During expansion, the film breaks, like a

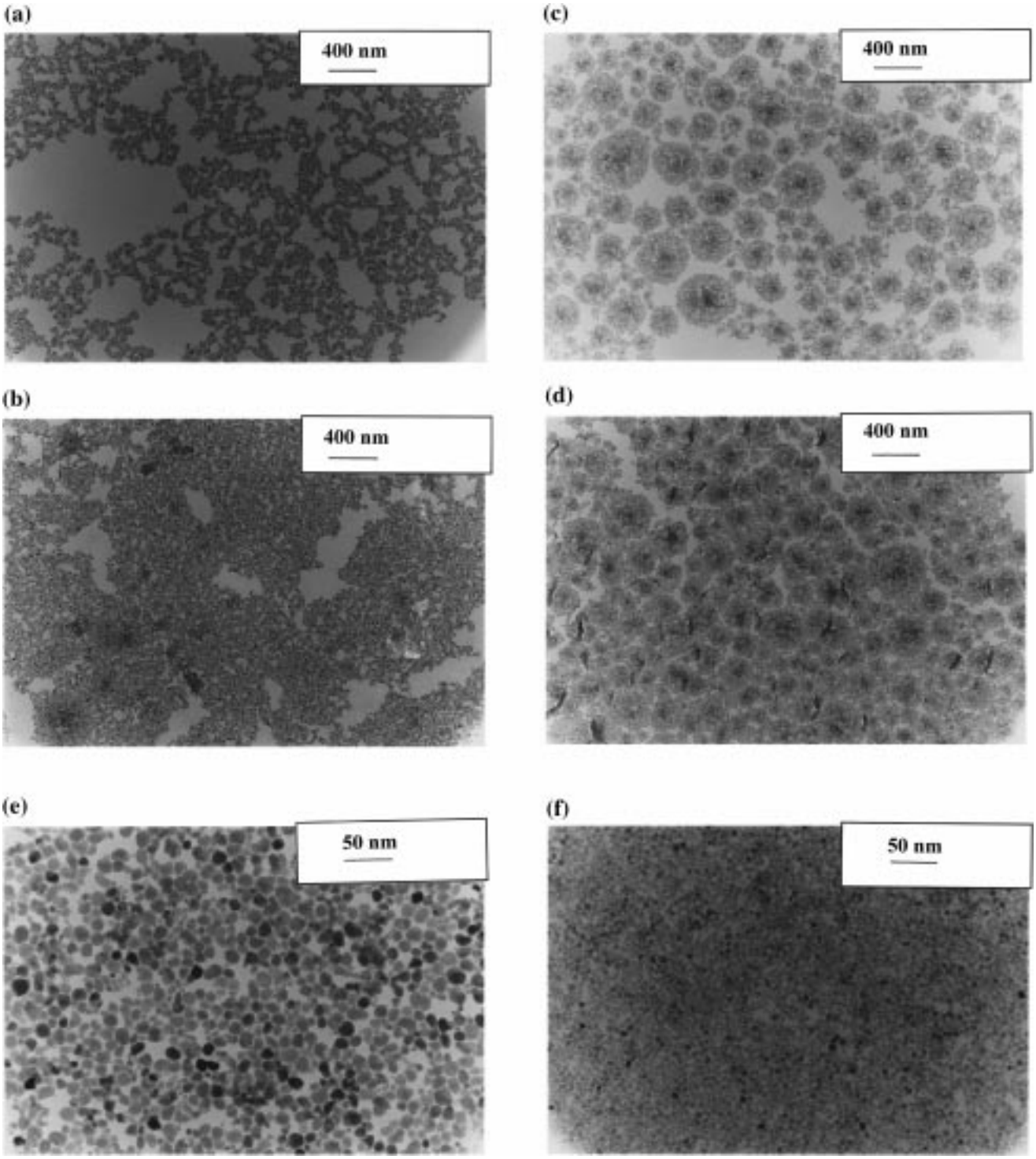

Figure 4. Electron micrographs. Parts a and b show 15.5-nm particles transferred at 5 and 14 mN/m, respectively. They form digitated aggregates. The bar length is 0.4 μm. Parts c and d show 7.5-nm particles transferred at 5 and 12 mN/m, respectively. In contrast to larger particles, they form dense circular compact aggregates. These are of the same magnification as that in parts a and b. Parts e and f show highly magnified images of 15.5- and 7.5-nm particle monolayers, respectively. The bar length in both cases is 50 nm.

rigid plate, into smaller pieces of homogeneous brightness (Figure 3b). After a compression−expansion cycle (Figure 3c), we no longer observe elongated aggregates, which also explains the nonreversibility of the first isotherm.

Electron Microscopy. To look at the film structure at the nanometric scale, the films have been tranfered onto an amorphous Formvar substrate at different pressures and have been imaged by electron microscopy. The shape of the domains is very different according to the particle size.

For 15.5-nm particles, at low pressure ($\Pi = 5$ mN/m), the particles are organized in long chains and form digitated aggregates (Figure 4a). When compressed, these aggregates become more compact, but even at the maximum of compression ($\Pi = 14$ mN/m), some porosity of the film is still noticeable (Figure 4b). In contrast, for 7.5-nm particles, both at low pressure ($\Pi = 5$ mN/m, Figure 4c) and at high pressure ($\Pi =$ 12 mN/m, Figure 4d), dense circular domains are observed in which the particles form a roughly compact arrangement. We did not succeed in transferring particles from a very low-pressure film ($\Pi = 0$ mN/m).

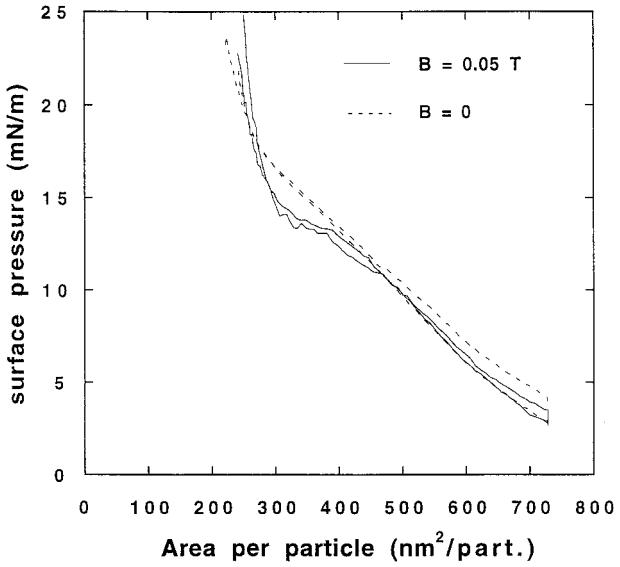

Figure 5. Isotherms $\Pi = f(A)$ for 15.5-nm particles submitted to a $B_\perp = 50$ mT magnetic field perpendicular to the film. A reference isotherm at $B_\perp = 0$ mT is also shown. The $B \neq 0$ surface-pressure decrease may be due to some reversible overlayering of particles (see text).

Parts e and f of Figure 4 are taken at higher magnification. The particles are clearly organized in a single monolayer. Notice the small diameter dispersity, especially for the 7-nm particles (Figure 4f).

We stress that these nanometric observations are not exactly similar to the ones reported at the micrometric scale. We think in fact that the nanometric structure is directly related to particle−particle interactions, while the micrometric one is probably more sensitive to interactions between domains on a larger scale.

Magnetic-Field Effect. This effect has been studied only for the largest particles, for which we expect the largest interaction with an external magnetic field.[10] When a $B_\parallel = 30$ mT field is applied parallel to the film, no clear and reproducible effect has been detected on the isotherm. At very low particle density ($A/A_0 \cong 10$), we have observed some alignment of the elongated aggregates along the field direction, but this effect was difficult to characterize because of the domain drift due to surface convection. On the other hand, when the $B_\perp = 50$ mT field is normal to the film, the isotherm shape is slightly modified, as illustrated in Figure 5; at high particle density, the magnetic field lowers the surface pressure by 1−2 mN/m. This process is completely reversible: when the field is switched off, one recovers the $B = 0$ isotherm.

Discussion

The first result of the present study is the important effect of the particle size on the isotherm shape. We already mentioned that the isotherms are reproducible except for the first compression−expansion cycle. This may be interpreted in two ways. First, some lauric acid in excess in the hexane ferrofluid may stay at the water−air interface during the deposition and solubilize in the subphase only during the first compression. Second, the first compression may induce some irreversible transformations in the 2D domains of particles. After deposition, we observed rigid domains digitated on the micrometric scale. They aggregate into larger ones during compression, and contact forces due to their geometry probably contribute to the surface pressure. Also, isolated particles in the gaseous state may irreversibly stick to large domains during this first step. During decompression, large domains break into smaller ones, but they remain compact (at least on the micrometric scale) and no longer appear digitated. Further cycles are no longer relative to the behavior of isolated particles but to the behavior of domains.

This last interpretation is supported by the way that the particle size modifies the isotherm shape. As a matter of fact, according to Figure 2, a film made of small particles appears more compressible than one made of larger particles, at least in the $A/A_0 > 1$ region. This is surprising because the attractive interactions between large particles are stronger than between small particles. These interactions are van der Waals and magnetic dipolar interactions. Both of them increase with particles size. In a naive description, large particles should constitute a more attractive system, thus more compressible than small ones. It is obviously not the case according to Figure 2. This contradiction disappears if one assumes that the isotherms reflect the behavior of domains and not of isolated particles. Then we can properly interpret the relative position of isotherms in terms of elasticity of domains, as discussed in the following.

Interactions between the particles are anisotropic because of the magnetic dipole−dipole term. This latter is strongly dependent on particle size and tends to align dipoles parallel to each other. For a dilute gas of particles (weak magnetic coupling), both magnetic and van der Waals interactions have the same $1/r^6$ behavior. According to ref 2, their ratio is larger than 1 for particles over 12 nm in diameter. Moreover, strong magnetic coupling occurs at short distance, since dipole alignment creates a nonzero local magnetic field. In a 3D gas of particles, numerical simulations have considered the balance between dipolar and isotropic interactions and its consequence for the stability of the colloidal system. When dipole−dipole interactions are strong enough, destabilization of the sol should lead to chained aggregates with aligned dipoles. But when isotropic interactions are dominant, gas−liquid-like transitions should be observed.[12] Two-dimensional simulations have also been performed by R. Pastor-Satorras et al. in ref 13. They compute the fractal dimension of 2D aggregates, D_H, as a function of the parameter $K^{-1} = D^3 k_B T/\mu^2$, where D is the particle diameter and μ its magnetic moment. They find that D_H is an increasing function of K^{-1}, and then of D^{-3}, since $\mu \sim D^3$. Our experimental results are thus in agreement with these numerical results, which predict that D_H is smaller for the larger particles. For the smaller particles ($D = 7.5$ nm) the agreggates are dense (D_H is close to 2), and for the larger ones ($D = 15.5$ nm) the aggregates are digitated ($1 < D_H < 2$).

The differences in the isotherms may now be understood by considering the different elastic behavior of these two kinds of domains, dense ones and digitated ones. For compact domains, contact forces are relevant only at high surface coverage. Thus, the surface pressure remains low when $A > A_0$ and rapidly increases when $A \cong A_0$, since the intrinsic compressibility of the domains is small. In contrast, for digitated domains the surface pressure increases as soon as the domains interpenetrate (this occurs at $A > A_0$), and the finite slope of the isotherm reflects their larger compressibility.

The fact that we do not observe the behavior of isolated particles, but of 2D aggregates, is in fact not so surprising. In magnetic fluids, a dispersion of surfactant-coated particles in an organic solvant is stabilized by steric repulsions, which depend on the solvent quality regarding the surfactant chain.[14] Phase transitions are anyway known to occur in such dispersions when the volume fraction of particles increases.[15] In hexane, diluted dispersions of surfactant-coated particles are thus stable,

and this stability is now well controlled. As soon as the hexane magnetic fluid is deposited on the water subphase, the solvent slowly evaporates and the volume fraction of particles is able to increase, leading to the creation of aggregates. Moreover, when the solvent is completely evaporated, the surfactant chains are no longer in a good solvent, and it is difficult to talk about steric repulsions. Thus, it is not surprising to observe irreversible aggregation.

The results in a magnetic field are only preliminary ones. In zero field, we think that the dipoles are parallel to the film surface, which lowers the dipolar energy. A strong enough field $B_{||}$ parallel to the surface should align the dipoles and decrease the surface pressure by $\Delta\Pi$; the expected order of magnitude for $\Delta\Pi$ is $-\mu B_{||}/A$, where $\mu \approx 10^{-19}$ A m^2 is the particle magnetic moment. At the maximum particle density, $|\Delta\Pi|$ is only on the order of 0.03 mN/m for $B_{||} = 30$ mT. This is below the sensibility of the surface pressure sensor, and one should increase the field intensity by about 1 order of magnitude to get a visible effect on the isotherm. We only observed some orientation of macroscopic elongated domains along the field, which gives support to the hypothesis of horizontal dipoles parallel to the domain axis.

Concerning the slight decrease of the surface pressure in a vertical field, we already mentioned that it is probably due to a reversible collapse of the film; a bilayer or a multilayer is the lowest-energy configuration for vertically oriented dipoles. However, this simple description does not take into account magnetic collective effects, and further experiments and modeling are necessary to characterize the interaction of the layer with a magnetic field.

Conclusion

A stable monolayer of hydrophobic monodisperse magnetic nanoparticles have been deposited on a water subphase. In this monolayer, the particles spontaneously form dense aggregates. The isotherm shape and the aggregate structure, revealed by electron microscopy, depend on the particle size. Larger particles form chained and rather compressible aggregates, although smaller particles form compact circular aggregates. This is consistent with the size-dependent balance between van der Waals and magnetic dipole−dipole interactions. Interactions with an external magnetic field B are expected to become important for $B > 100$ mT.

Acknowledgment. The authors are greatly indebted to M. Lavergne who produced the electron micrographs in the Groupement Régional de Mesures Physiques (Université Pierre et Marie Curie). M.A. gratefully acknowledges support from a European Community fellowship (Human Capital and Mobility Program).

References and Notes

(1) Fabre, P.; Casagrande, C.; Veyssie, M.; Cabuil, V.; Massart, R. *Phys. Rev. Lett.* **1990**, *64*, 539.

(2) Ménager, C.; Belloni, L.; Cabuil, V.; Dubois, M.; Gulik-Krzywicki, T.; Zemb, Th. *Langmuir* **1996**, *12*, 3516.

(3) Ménager, C.; Cabuil, V. *Colloid Polym. Sci.* **1994**, *272*, 1295.

(4) Hervé, P.; Nome, F.; Fendler, J. H. *J. Am. Chem. Soc.* **1984**, *106*, 8291.

(5) Bacri, J. C.; Perzynski, R.; Salin, D.; Cabuil, V.; Massart, R. *J. Magn. Magn. Mater.* **1990**, *85*, 27.

(6) Bacri, J. C.; Perzynski, R.; Salin, D.; Cabuil, V.; Massart, R. *J. Colloid Interface Sci.* **1989**, *132* (1), 43.

(7) Meldrum, F. C.; Kotov, N. A.; Fendler, J. H. *J. Phys. Chem*. **1994**, *98*, 4506.

(8) Massart, R. *IEEE Trans. Magn.* **1981**, *17*, 131.

(9) Dubois, E.; Cabuil, V.; Massart, R.; Hasmonay, E.; Perzynski, R. *J. Magn. Magn. Mater.* **1995**, *149*, 1.

(10) Bacri, J.-C.; Cabuil, V.; Massart, R.; Perzynski, R.; Salin, D. *J. Magn. Magn. Mater*. **1986**, *62*, 36.

(11) Flament, C.; Gallet, F. *Mod. Phys. Lett. B* **1995**, *9*, 1791.

(12) Van Leeuwen, M. E.; Smit, B. *Phys. Rev. Lett.* **1993**, *71* (24), 3991.

(13) Pastor-Satorras, R.; Rubi, J. M. *Phys. Rev. E* **1995**, *51* (6), 5994.

(14) Jansen, J. W.; de Kruif, C. G.; Vrij, A. *J. Colloid Interface Sci.* **1986**, *114* (2), 471. Jansen, J. W.; de Kruif, C. G.; Vrij, A. *J. Colloid Interface Sci.* **1986**, *114* (2), 481.

(15) Pusey, P. N. *Liquides, Cristallisation et Transitions Vitreuses*, Les Houches 1989, Session LI; Hansen, J. P., Lesveque, D., Zinn-Justin, J., Eds.; Elsevier Science: North Holland, Amsterdam, 1990; Part II, p 765.